

---

# Material Informatics through Neural Networks on Ab-Initio Electron Charge Densities: the Role of Transfer Learning

---

Dario Massa<sup>\*1,2</sup> Stefanos Papanikolaou<sup>2</sup> Piotr Sankowski<sup>1</sup>

## Abstract

In this work, the dynamic realms of Materials Science and Computer Science advancements meet the critical challenge of identifying efficient descriptors capable of capturing the essential features of physical systems. Such task has remained formidable, with solutions often involving ad-hoc scalar and vectorial sets of materials properties, making optimization and transferability challenging. We extract representations directly from ab-initio differential electron charge density profiles using Neural Networks, highlighting the pivotal role of transfer learning in such task. Firstly, we demonstrate significant improvements in regression of a specific defected-materials property with respect to training a deep network from scratch, both in terms of predictions and their reproducibilities, by considering various pre-trained models and selecting the optimal one after fine-tuning. The remarkable performances obtained confirmed the transferability of the existent pre-trained Convolutional Neural Networks (CNNs) on physics domain data, very different from the original training data. Secondly, we demonstrate a saturation in the regression capabilities of computer vision models towards properties of an extensive variety of undefected systems, and how it can be overcome with the help of large language model (LLM) transformers, with as little text information as composition names. Finally, we prove the insufficiency of open-models, like GPT-4, in achieving the analogous tasks and performances as the proposed domain-specific ones. The work offers a promising avenue for enhancing the effectiveness of descriptor identification in complex physical systems, shedding light over the power of transfer learning to easily adapt and combine

available models, with different modalities, to the physics domain, at the same time opening space to a benchmark for LLMs capabilities in such domain.

## 1. Introduction

Machine Learning (ML) has initiated a remarkable transformation in Materials Science, with the emergence of Materials Informatics (MI) (Ramakrishna et al., 2019; Ramprasad et al., 2017; Takahashi & Tanaka, 2016; Ward & Wolverton, 2017; Rajan, 2005) playing a pivotal role in shaping the forefront of innovation in recent years. This field has become crucial in accelerating materials discovery by deploying ML techniques (Michalski et al., 2013; LeCun et al., 2015) in various contexts, for example including the exploration of carbon-capture (Lin et al., 2012; Wilmer et al., 2012) and organic materials (Montavon et al., 2013; Rupp et al., 2012b), as well as materials for electrocatalysis (Hong et al., 2016; Greeley et al., 2006).

A usual challenge in the proposed context is the identification of efficient descriptors, capable of grasping the essential features of complex physical systems. In the context of materials simulations, a wide variety of descriptors have been proposed, both based on translationally and rotationally invariant functions of atomic coordinates (Rupp et al., 2012a; Behler, 2011; Pietrucci & Andreoni, 2011; De et al., 2016; Sadeghi et al., 2013), or involving fixed-length feature vectors of atomic or electronic properties (Seko et al., 2015; Xue et al., 2016; Isayev et al., 2017). Even if powerful, the proposed descriptors are constructed on the basis of the systems they are applied on, leading to a careful ad-hoc design of their components.

The idea of using neural network architectures to extract representations directly and flexibly has nowadays made a remarkable step also in the field of Materials Science, for example with the aim of Graph Convolutional Neural Networks (GCNNs) for the prediction of properties in systems ranging from crystals (Xie & Grossman, 2018a;b; Chen et al., 2019; Dunn et al., 2020), surfaces (Back et al., 2019), or molecules (Jorgensen et al., 2018; Schütt et al., 2017; Duvenaud et al., 2015; Wu et al., 2018). Their use

---

<sup>1</sup>IDEAS-NCBR Chmielna 69 00-801 Warsaw, Poland.  
<sup>2</sup>NOMATEN Center of Excellence in Multifunctional Materials, ul. Andrzeja Sołtana, 05-400 Otwock, Świerk, Poland.. Correspondence to: Dario Massa <dario.massa@ideas-ncbr.pl>, Piotr Sankowski <piotr.sankowski@ideas-ncbr.pl>.

can present strong advantages with respect to classical approaches, but require large amounts of data to be trained on. Wide open-source databases (Saal et al., 2013a; Jain et al., 2013; Curtarolo, 2012; Hachmann et al., 2011) originated from high-throughput (Curtarolo et al., 2013; Saal et al., 2013b) ab-initio Density-Functional-Theory (DFT) (Kohn et al., 1996; Cohen et al., 2012) calculations represent the key ingredient for the development of such models, and of MI in general. However, available material databases can clearly lack of physically meaningful materials configurations, like in the presence of local or extended defects, or metastable configurations belonging to relaxation or reaction processes, which imply the need of the trained models of extrapolation, rather than interpolation, for their properties. One of the possible proposed solutions towards applicability to arbitrary structures, is the building of extended datasets of very diverse materials structures, including for example high temperature configurations (Takamoto et al., 2022).

In this work, we propose the extraction of efficient representations for materials directly from their ECD profiles, which are supposed to encode the necessary information regarding their properties, in terms of constitutive atoms and their interactions, and regardless of dimensionality, stability, and compositions. In Section 2, we introduce one of the tentatives that has been done in this direction, in the particular case of training from scratch CNNs for regression tasks on ECD images in the presence of defects (Arora et al., 2022). Using the available data for this example, we prove the importance of introducing Transfer Learning (TL) techniques (Torrey & Shavlik, 2010), which lead to significant improvements in performances and reproducibility on the same task. Taking advantage of the large dataset of electron densities on the Materials Project (MP) (Jain et al., 2013) database, we also demonstrate the possibility of performing regression tasks over a large variety of materials, and, by contrast with the aforementioned case, the role of defects in the latter in facilitating the features extraction. Finally we show the improvements that can arise by adding text as additional input information, as well as the insufficiency of open-models like GPT-4 (OpenAI et al., 2023) in achieving the good performances of the proposed domain-specific models. The study proposes a focus on the non-trivial learning of extended physics-domain data and relations through TL techniques, allowing efficient representations extraction without ad-hoc functional building or database design, even in the case of small sets. It also sheds light on the power of multimodal physics-aware models and databases, opening the space for a benchmark of LLMs in such domain.

## 2. Related Work

**Regression task with CNNs on density images** G. Arora et al. (2022) trained from scratch a CNN on planar ECD images to predict energy values of defected crystals. In particular, they predict the Stacking Fault Energy (SFE), a measure of the excess energy associated to irregularities in the sequence of planes in crystals (Shih et al., 2021), focusing on Ni-based alloys, in which the alloying element sits at the interesting fault plane. A small dataset of 137 colored planar ECD images, extracted in correspondence of the defect, is used to train a CNN model to predict the induced changes in the SFE.

**Unsupervised approach** D. Massa et al. (2023) demonstrated the power of defect-induced electron charge density perturbations by means of unsupervised learning techniques, in the context of hydrogen interstitials in metals. Their analysis uncovers strong correlations between (I) density-based descriptors properties and atomic properties of pristine bulks (PBs) (i.e. bonding radius, lattice constants) and (II) hydrogen Bader charge volumes with PBs macroscopic (i.e. melting point, heat of formation) and structural (i.e. Bulk modulus) properties. Charge response categories emerge, also connecting to hydrogen diffusion barriers in the different host crystals, as validated via ab-initio Nudge-Elastic-Band calculations.

**Multimodal neural networks** Multimodal neural networks (Summaira et al., 2021) harness the capacity to integrate and process information from diverse sources, such as text and images. The Contrastive Language-Image Pre-training (CLIP) model from OpenAI (Radford et al., 2021), represents a pioneering example in the field, being capable of transfer and compete zero-shot in image recognition tasks with well known fully supervised baselines like ResNet-50 on ImageNet. GPT-4 is also an excellent example of multimodal open models, which has demonstrated heightened proficiency in generating coherent and contextually relevant text, as well as human-level performance on professional and academic benchmarks (OpenAI et al., 2023).

**A database for electron charge densities** The Materials Project (Jain et al., 2013) has included in its database 122 690 ab-initio electron charge densities, which can be retrieved thanks to their API. To our knowledge, the MP database is the first and only containing this kind of volumetric data associated to materials properties, and in this regard is worth mentioning the work of Shen et al. in developing a dedicated tool, Py-Rho (2021), capable of efficiently manipulating the density grids.

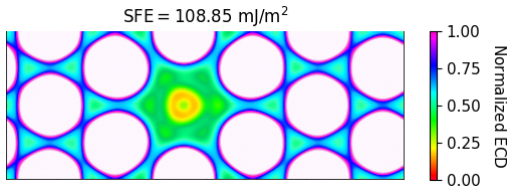


Figure 1. Example of input ECD image from the dataset of Arora *et al.* (2022). A SFE value is associated to each ECD image, and used to train from scratch the CNN model in Table(1) for the prediction of the same target quantity in unseen data.

### 3. Methods

#### 3.1. The reference model and its dataset

As explained in Sec.(1,2), we first focus on the results of the work from G. Arora *et al.* (2022) and their CNN model, which has been trained from scratch on a small dataset of ECD planar images for a regression task on SFE energies in Ni-based alloys. The dataset is composed of 137 colored images of size  $196 \times 75 \times 3$  extracted performing DFT simulations, and is divided in 80% for training, 10% for validation and 10% for holdout. The planar images containing the ECD isolines are extracted at the stacking-fault plane, where substitutional defects from 3d, 4d and 5d series sit in different concentrations to simulate the effects of alloying in inducing changes in the SFE values. For further details regarding the computer simulations performed by the authors and samples related choices, we redirect the reader to the reference work (Arora *et al.*, 2022).

An example of input data sample and the model architecture are reported respectively in Fig.(1) and Table(1), and consists of a sequence of layers involving an Input layer, 2D Convolutional and Average Pooling layers, Dropout, Flatten and Dense layers. The images are fed in batches of 8, early stopping is applied with a patience of 50 epochs on accuracy, and learning rate with Adam optimizer is set to 0.0007. The model performances are evaluated via Root Mean-Squared Error (RMSE) and the  $R^2$  coefficient of determination. All RMSE values referred to this proposed context are intended to be in  $mJ/m^2$ , as they inherit the units of the computed SFEs.

#### 3.2. Transfer learning techniques with CNNs

We introduce TL techniques for the same regression problem proposed by G. Arora *et al.* (2022).

**Pre-trained models** A number of pre-trained models is considered, to evaluate their performances on the small dataset of 137 ECD images: InceptionV3, Xception, VGG16, VGG19 and DenseNet121, in their configurations trained on ImageNet. Each model is imported through the Keras (Chol-

et *et al.*, 2015) library, without including top-layers, and freezing the rest of their architectures, adding and training a custom regression head involving a GlobalAveragePooling2D layer, a Dropout layer with frequency 0.2, and a single Dense neuron. The performances of the models are evaluated according to the same measures of the reference work.

**Fine-tuning** After preliminary experiments on performances, involving k-fold validation and data augmentation, a best model is selected for fine-tuning (FT), during which the architecture layers are gradually unfrozen. The details of such explorations will be presented in the Experimental Results Section.

#### 3.3. A larger and multimodal density dataset

As anticipated in Sec.(1), the Materials Project database has included ECDs for a large subset of its samples, which can be retrieved thanks to the available API, together with target materials properties. Such samples represent a very diverse collection of bulk crystals in terms of compositions (pure and multi-component), symmetries and energetics.

For the building of a dataset of such undefected systems, we first filter all the stable face-centered cubic (FCC) crystals, collect their MP-IDs and the associated target properties in a Pandas Dataframe, focusing on the scalar attributes only. Among all the available materials properties, we filter out the ones that, in the collected subset, show missing values (NaNs), resulting in a final set of 785 entries and 25 target features. The list of scalar properties associated with the ECDs is reported in Table(11) of the Appendix. Particular interest is devoted to energy band gaps ( $E_{BG}$ ), formation energies ( $E_F$ ), total magnetizations ( $M_{tot}$ ) and bulk moduli (B), for which we report the distributions in Fig.(6) of the Appendix. As it can be noticed, the majority of samples is represented by ternary crystals; quantum-level characterization of such materials is very demanding from a computational point of view, and a predictive model of their properties based on available databases is highly desirable.

With the help of the Robocrystallographer (Ganose & Jain, 2019), a tool capable of generating text descriptions of crystalline structures by analyzing their symmetry, local environment, and extended connectivity, we build a Dataframe of text attributes associated to each MP-ID, example of which is reported in Table(2). We stress here that such descriptions can be generated just by feeding the Robocrystallographer with the Pymatgen structures of the systems of interest. In order to test how and in which measure the provided text can contribute to the performances, we consider the different cases of text containing i) a single word, namely the crystal composition, ii) some key text, involving crystal composition and bonding lengths and iii) all the allowed input text for the LLM in consideration. We finally build

Layer	Output	Parameters
Input-1 (InputLayer)	[(None, 73, 196, 3)]	0
Conv2d-1 (Conv2D)	(None, 72, 195, 32)	416
Conv2d-2 (Conv2D)	(None, 71, 194, 64)	8256
Average pooling-1 (AveragePooling)	(None, 35, 97, 64)	0
Conv2d-3 (Conv2D)	(None, 34, 96, 96)	24,672
Conv2d-4 (Conv2D)	(None, 33, 95, 192)	73,920
Average pooling-2 (AveragePooling)	(None, 16, 47, 192)	0
Conv2d-5 (Conv2D)	(None, 15, 46, 192)	147,648
Dropout-1 (Dropout)	(None, 15, 46, 192)	0
Conv2d-6(Conv2D)	(None, 14, 45, 256)	196,864
Average pooling-3 (AveragePooling)	(None, 7, 22, 256)	0
Conv2d-7 (Conv2D)	(None, 6, 21, 256)	262,400
Flatten-1 (Flatten)	(None, 32,256)	0
Dense-1 (Dense)	(None, 32)	1,032,224
Dense-2 (Dense)	(None, 1)	33
		Tot: 1746
		Trainable: 4331746
		Non Trainable: 4330

Table 1. Model architecture of the CNN proposed in the reference work (Arora et al., 2022).

MP-ID	mp-72
Description (All)	Ti crystallizes in the hexagonal P6/mmm space group. There are two inequivalent Ti sites. In the first Ti site, Ti(1) is bonded in a 14-coordinate geometry to two equivalent Ti(1) and twelve equivalent Ti(2) atoms. Both Ti(1)-Ti(1) bond lengths are 2.83 Å. All Ti(1)-Ti(2) bond lengths are 2.99 Å. In the second Ti site, Ti(2) is bonded in a 11-coordinate geometry to five equivalent Ti(2) and six equivalent Ti(1) atoms. There are three shorter (2.64 Å) and two longer (2.83 Å) Ti(2)-Ti(2) bond lengths.
Description (Single)	Ti
Description (Key)	Ti. Both Ti(1)-Ti(1) bond lengths are 2.83 Å. All Ti(1)-Ti(2) bond lengths are 2.99 Å.

Table 2. An example of text description for a MP sample (Ti) in the multimodal dataset.

Dataframes of the ECDs, by interrogating the API whether the collected MP-IDs are accompanied with a density field. Out of the previously collected IDs, 781 satisfy the request. Each ECD field comes from ab-initio simulations, in which the resulting datagrids dimensions may differ from case to case, depending on the system and parameters of interest. For this reason, we exploit the dedicated Py-Rho regridding tool, unifying the grid dimensions to  $60 \times 60 \times 60$ . Also, even though both total and differential ECDs are available, we focus on the latter, for the enhanced variability within and among samples originating from the highlighting of interatomic interactions, rather than local atomic electron densities. A comparison between slices along the z-axis of total and differential ECD fields is presented in Fig.(2).

As it can be noticed from the collection of slices, even though the differential ECD fields are to be preferred, their remarkable variability within a sample may represent a source of confusion when it comes to the desirable association with a specific material and its properties, in the presence of a large set of systems. For this reason, we decided to focus on a single slice of the available volumetric data, which could be considered as representative for the subset. Given the restriction to FCC symmetry, we systematically extract from each volume the planar data belonging to the  $\langle 111 \rangle$  plane, known to be characterized by the larger atomic density in such symmetry. In Fig.(3), we show an example of the result of this procedure.

In conclusion, the available data for a multimodal regression task is composed by three datasets, in which to each MP-ID a flattened 2D ECD field is associated, as well as the scalar properties and text descriptions of the material it comes from.

### 3.4. Transfer learning with text: a custom multimodal model

In order to exploit different kind of data, as text and images, a custom regression model able to assimilate both is needed. As mentioned in Sec.(2), the Contrastive Language-Image Pre-training (CLIP) model from OpenAI (Radford et al., 2021) is an example of a multimodal model using natural language supervision for image representation learning, ultimately connecting the two modalities in a shared embedding space. Considering natural language as a training signal, Radford *et al.* proved the importance of the resulting direct bridging of the learned representations to language, which enabled remarkable zero-shot transfer performances of the model. However, since our objective is to assess the performance enhancement in a regression task for materials properties, by incorporating textual information into a conventional image-only transfer learning framework, similar to the one outlined in Sec.(3.2), we decided to base the building of the custom multimodal model as a continuation

of the latter.

Specifically, after fine-tuning the best resulting model on an image-only dataset, we deploy it once again, assuming it to be a new pre-trained model on which performing the same transfer-learning procedure previously described. A custom model is built, adding the possibility of concatenating text embeddings, obtained from the application of Large Language Models (LLMs) on the text data, with features extracted from the image data with the new pre-trained model. For this task, RoBERTa (Liu et al., 2019) and ALBERT (Lan et al., 2019) are used, trying to evaluate the importance of the complexity of the model, as well as of the length of the text descriptions imported. An example of the resulting model architecture is reported in Table(3).

## 4. Experimental Results

### 4.1. Improving the reference work with TL

In this Section, we aim at proving the importance of TL techniques for CNN models towards the domain of physics-derived data, like ECD fields, especially in the presence of small datasets. As anticipated in Sec.(2.3.1), in the reference work for comparison (Arora et al., 2022), the authors focus on a regression task on SFE using a custom CNN model trained from scratch on ab-initio planar ECD images. The reported performances in terms of  $R^2$  are of 0.98, 0.88 and 0.87 respectively on the training, validation and holdout sets. The original dataset is composed by 137 2D images of the ECD isolines, extracted at the SF plane of Ni-based alloys, where the alloying element sits.

As a first point, we would like to focus on the limitations of the reference CNN model. In the presence of little data, it is common practice to introduce techniques like data augmentation and K-fold validation to avoid overfitting. The model proposed by the authors, whose architecture has been presented in Table(1), lacks of such tools, providing a sub-optimal solution to the problem it aims to solve, as proved by a brief reproducibility test. In Fig.(5) and Table(8) of the Appendix, we report the results of running the original code on the original dataset (Arora) for different trials, finding low performances on the test and holdout sets.

In order to implement a TL approach in the proposed context, we decided to keep the same image dimensions as in the original work (Arora et al., 2022), but splitting the data in 70% for training, 15% for validation and 15% as holdout. As explained in Sec.(3.1), we import a number of available pre-trained model in Keras, freezing their architecture and considering a custom trainable regression head. We manually test different batch sizes, ranging from 4 to 12 with a step of 2, and for each we treat the learning rate (LR) as an hyperparameter, through Keras Tuner (O'Malley et al., 2019). We introduce data augmentation, including a Ran-

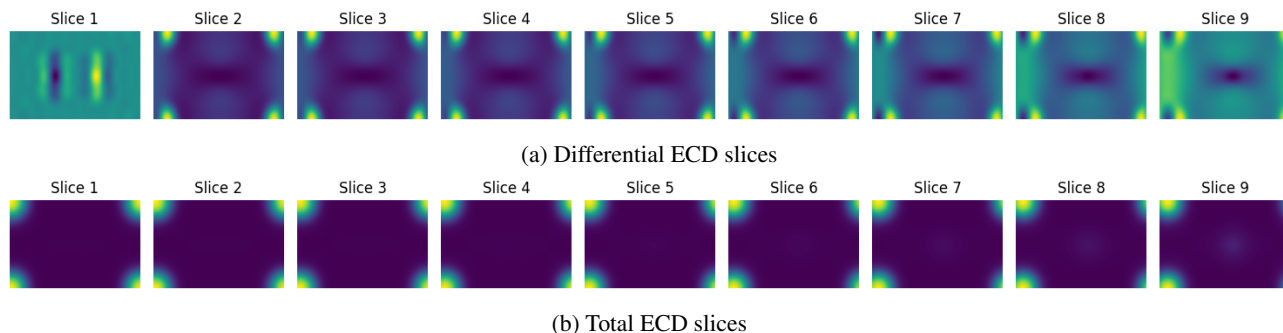


Figure 2. An example of 2D slices along the z-axis of the ECD volumetric data for an MP sample (mp-72, Ti).

Layer (type)	Output Shape	Param
input_ids (InputLayer)	[(None, 100)]	0
attention_mask (InputLayer)	[(None, 100)]	0
tf_roberta_model (TFRobertaModel)	ast_hidden_state=(None, 100, 768), pooler_output=(None, 768), past_key_values=None, hidden_states=None, attentions=None, cross_attentions=None	124,645,632
input_12 (InputLayer)	[(None, 75, 75, 3)]	0
average_pooling1d (AveragePooling1D)	(None, 1, 768)	0
model_4 (Functional)	(None, 1)	21,804,833
flatten (Flatten)	(None, 768)	0
concatenate (Concatenate)	(None, 769)	0
dense_11 (Dense)	(None, 32)	24,640
dropout_48 (Dropout)	(None, 32)	0
dense_12 (Dense)	(None, 1)	33
		Tot.: 146,475,138 Trainable: 24,673 Non-trainable: 146,450,465

Table 3. Custom multimodal model, layers and parameters.

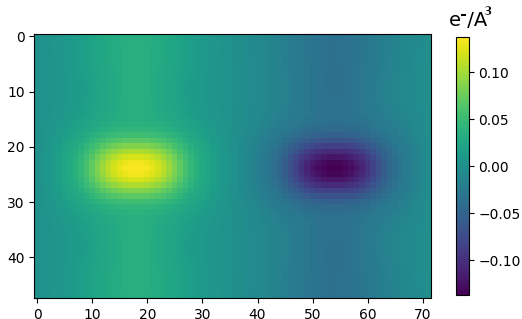


Figure 3. Example of a 2D slice from the differential ECD volumetric data for the mp-72 (Ti) sample, along the  $\langle 111 \rangle$  plane.

domFlip layer with horizontal and vertical flipping, and a RandomRotation layer with frequency of 0.2. Dealing with a small dataset, we also introduce K-fold validation with  $K = 10$ , and control best and average performances over the folds. During training of the last custom layers, we monitor the validation loss, introducing an early stopping with a patience of 10 epochs. The performances of the models are evaluated according to the same measures of the reference work, and are reported for their best parameters in Table(4).

As it can be noticed, among the selected models, in absence of fine-tuning the InceptionV3 reports the highest scores on all sets, with an  $R^2$  value of 0.9 (training set) and 0.89 (test set and holdout set), which already surpassed the reference work in terms of its generalizations capabilities. It is interesting to notice the remarkable change in the order of magnitude of the best selected LR for the specific models considered: the overall performances for the regression task anti-correlate with the magnitude of the best LR for the specific models. In the context of TL, a low learning rate is generally desirable to allow adaptation to the new data without the loss of prior knowledge, and we find confirm in the best performances for a model showing a preferred low LR.

For the fine-tuning stage on InceptionV3, we try a gradual unfreezing of the higher layers of the model, starting with the first 50, recompiling the model with  $LR = 0.0001$  and training it keeping the same optimal batch size and early-stopping procedure. The first fine-tuning stage is the one that leads to the best improvements in performances, with a variable increase in  $R^2$  value up to 6% during trials, while we observe gradual degradation in performances if deeper unfreezing stages are considered. Tables(9,10) in the Appendix report the stability tests of the fine-tuning improvement under slight changes in the learning rate and on different computing machines, with no seed fixing. Finally, for the sake of reproducibility, we fix the seed in the computation, and propose a final performance improvement due to the fine-tuning procedure in Table(5) and Fig.(4).

## 4.2. The multimodal approach on electron densities

As explained in Sec.(3.4), we aim at testing the performances of a combined CNN and LLM model on the multimodal dataset made of images and generated text, in the regression towards properties of a variety of undefected bulk crystals. For this purpose, we focus on the best performing InceptionV3 model for the extraction of features from ECD images, and consider RoBERTa for the extraction of features from the generated text about crystals.

During experiments, we explore the application of the developed multimodal model for regression of different target materials properties, namely energy band gap ( $E_{BG}$ ), formation energy ( $E_F$ ), total magnetization ( $M_{tot}$ ) and bulk modulus (B). Such properties typically involve expensive quantum-level simulations (i.e. DFT) in order to be accurately computed, therefore a predictive model is highly desirable for them.

Table(6) reports the performances of the finetuned multimodal InceptionV3+RoBERTa model on top of the finetuned InceptionV3 model only, in the case of Single word, Key words, or All words allowed by the model. It is worth mentioning that in the comparison among different regression targets and different amount of support text, the hyperparameter space has not been explored, but kept fixed to the optimal values found in the previous sections for the InceptionV3 model.

The best overall performances of the multimodal model are found in the Key words case, containing the crystal composition and bond-lengths information, in particular for the prediction of the bulk modulus and formation energy, respectively with remarkable  $R^2 = 0.91$   $R^2 = 0.86$  on the Holdout set. The predictions over band-gaps and total magnetizations suffer from overfitting, possibly due to the unchanged parameters setting, or unbalanced distributions towards zero-valued properties<sup>1</sup>, but show interesting potential. In comparison with the predictions supported by a Single word text information, namely crystal composition, it can be understood that the largest improvement is obtained for the band-gap prediction, for which more than 20% score is gained on the Holdout set. In Table(13) and Fig.(7) of the Appendix, we report an example of the gradual improvement of performances during the multiple transfer learning stages, involving finetuning of the InceptionV3 and finetuning of the InceptionV3+RoBERTa. Interestingly, and conversely with respect to the dataset of defected systems previously analysed in Sec.(4.1), the finetuning of InceptionV3 model only cannot achieve good regression performances in the case of undefected materials: a low-score saturation is observed, which gets overcome with the addition of text extracted features. By looking at the All words case instead,

<sup>1</sup>Pronounced by the restriction to the FCC symmetry only.

Model	Param.	Training		Testing		Holdout	
		BS , LR	RMSE	R <sup>2</sup>	RMSE	R <sup>2</sup>	RMSE
InceptionV3	6 , 0.007	4.83	0.9	5.33	0.89	5.87	0.89
Xception	4 , 0.05	6.52	0.81	8.26	0.72	5.97	0.88
VGG16	8 , 0.12	10.31	0.53	11.1	0.5	9.39	0.71
VGG19	8 , 0.34	10.67	0.5	11.84	0.43	10.07	0.66
DenseNet121	4 , 0.05	10.53	0.51	11.04	0.51	8.85	0.74

Table 4. Comparison between the different models performances (no fine-tuning).

Model	Param.	Training		Testing		Holdout	
		BS , LR	RMSE	R <sup>2</sup>	RMSE	R <sup>2</sup>	RMSE
InceptionV3 (before FT)	6 , 0.0070	7.47	0.75	7.58	0.77	7.37	0.82
InceptionV3 (after FT)	6 , 0.0070	5.84	0.85	4.63	0.91	4.73	0.93

Table 5. Performances of the fixed seed proposed model after fine-tuning.

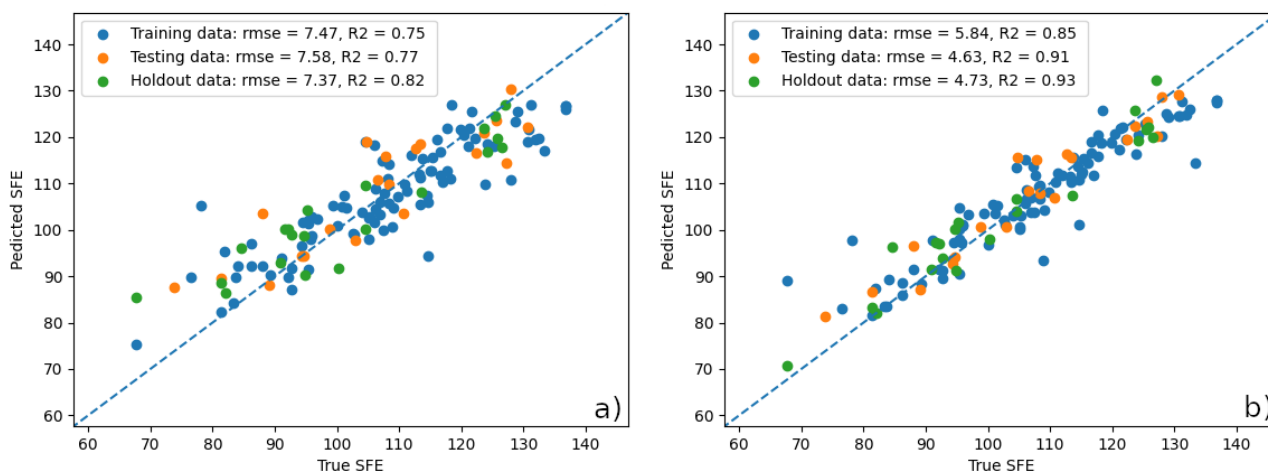


Figure 4. a) Performances of the model before finetuning, on the training, test and holdout portions of the dataset. b) Performances of the model after finetuning.

Target	Measure	roberta-base								
		Single			Key			All		
		Tr	Te	H	Tr	Te	H	Tr	Te	H
E <sub>BG</sub>	RMSE (eV)	0.06	0.09	0.09	0.02	0.07	0.07	0.03	0.08	0.08
	R <sup>2</sup>	0.73	0.50	0.45	0.96	0.71	0.68	0.90	0.60	0.54
E <sub>F</sub>	RMSE (eV/atom)	0.06	0.07	0.07	0.04	0.05	0.06	0.03	0.05	0.07
	R <sup>2</sup>	0.87	0.82	0.81	0.95	0.88	0.86	0.97	0.89	0.83
M <sub>tot</sub>	RMSE (μB)	0.02	0.04	0.09	0.02	0.04	0.10	0.02	0.04	0.10
	R <sup>2</sup>	0.94	0.75	0.57	0.92	0.79	0.52	0.94	0.80	0.50
B	RMSE (GPa)	0.03	0.05	0.05	0.04	0.04	0.04	0.04	0.05	0.04
	R <sup>2</sup>	0.96	0.86	0.88	0.92	0.92	0.91	0.93	0.88	0.91

 Table 6. Comparison between the performances of the custom combined model of InceptionV3 and RoBERTa (in the roberta-base version) for regression of crystal properties using images and text, in the case of Single word (crystal composition), Key words (composition and bond lengths) and of All words allowed by the model. The target properties for regression are: energy band gap (E<sub>BG</sub>), formation energy (E<sub>F</sub>), total magnetization (M<sub>tot</sub>) and bulk modulus (B). Performances are evaluated in terms of RMSE and R<sup>2</sup> measures, for training (Tr), testing (Te), and Holdout (H) sets.



the results seem to suggest that when the remaining words are included in the dataset, no improvement is gained.

### 4.3. Tackling the adequacy of open-models

As a last experiment, the performances of an open multimodal model like GPT-4 (OpenAI et al., 2023) in the same multimodal regression task previously introduced, are explored. To do so, the API is exploited, defining the role that the model shall assume during the request, namely a predictor of a target material property associated with a given ECD image and text description, after few in-context examples of such triad are presented to it. After considering the same data and splitting as for the domain-specific models investigations above presented, the in-context examples are initially shown to the GPT-4 belong to the training dataset, while the subsequent validation of its predictions happens on the holdout portion.

The results of such experiments are presented in Table(7), and deliver a marked discrepancy with what has been observed, i.e. in Table(6), for the corresponding task performed by custom domain-specific models. In particular, after observing 5 in-context examples of the triad of ECD image, single word text description (composition names) and target value, i.e. of B, the GPT-4 RMSE(GPa) of 0.16 stands against the 0.05 achieved with the combined multimodal model of InceptionV3 and RoBERTa. Such finding proves that: i) even though GPT-4 is one among the most advanced multimodal open models available nowadays, the latter are not yet ready, without proper finetuning, to generalize to domain-specific tasks from the physics realm, at list when the vision modality is present; ii) there is still need for research on domain-specific models, as well as for multimodal datasets on which instead open-models can be benchmarked to look for improvements.

## 5. Conclusion

In conclusion, our study has illuminated a remarkable approach to extract materials descriptors from electron charge densities through the lens of machine learning, emphasizing the efficacy of transfer learning in both defected and undefected bulk crystals of various complexity in terms of composition. We have demonstrated the significance of defects in facilitating the extraction of features, leveraging local highlights in charge density images, as well as of having a dataset of materials in which such defects live inside the very same host crystalline matrix, even though in different concentrations. Clearly, it is the case that a richer database, both in terms of number of samples and greatly varying materials compositions and properties, represents a harder target for regression. However, notably, our findings underline the pivotal role of textual information, such as composition names or key crystallographic details, in over-

coming performance saturation observed in the absence of defects. Finally, we proved the inadequacy of open-models in performing zero-shot predictions on the same multimodal datasets provided to domain-specific multimodal models, also in the presence of multiple in-context examples. Such evidence shall bring back the focus on the importance of physics-aware models and databases, and on the importance of a benchmark for LLMs in such domain, of which this work provides a first example.

Overall, our exploration contributes to the awareness of the strong potential of transfer learning within the realm of computer vision, showcasing the versatility of multimodal models. Indeed, applications of such models in physics are potentially extensive, as they can effectively harness any meaningful descriptive signal related to target material properties. This research not only provides a concrete example of how to efficiently perform regression tasks over material properties but also highlights the broader implications of the approach, paving the way for future advancements at the intersection of machine learning and materials science.

## References

- Arora, G. Dft\_stacking\_fault\_energy. [https://github.com/Materials-Computation-Data-Science-MCDC/DFT\\_Stacking\\_Fault\\_Energy](https://github.com/Materials-Computation-Data-Science-MCDC/DFT_Stacking_Fault_Energy).
- Arora, G., Kamrava, S., Tahmasebi, P., and Aidhy, D. S. Charge-density based convolutional neural networks for stacking fault energy prediction in concentrated alloys. *Materialia*, 26:101620, 2022.
- Back, S. et al. Convolutional neural network of atomic surface structures to predict binding energies for high-throughput screening of catalysts. *J. Phys. Chem. Lett.*, 10:4401–4408, 2019.
- Behler, J. Atom-centered symmetry functions for constructing high-dimensional neural network potentials. *The Journal of chemical physics*, 134(7), 2011.
- Chen, C. et al. Graph networks as a universal machine learning framework for molecules and crystals. *Chem. Mater.*, 31(9):3564, 2019.
- Chollet, F. et al. Keras. <https://keras.io>, 2015.
- Cohen, A. J., Mori-Sánchez, P., and Yang, W. Challenges for density functional theory. *Chemical reviews*, 112(1): 289–320, 2012.
- Curtarolo, S. A distributed materials properties repository from high-throughput ab initio calculations. *Comput. Mater. Sci.*, 58(227), 2012.

In-Context samples	Text info	Feature	RMSE	R <sup>2</sup>
5	Single	B (GPa)	0.16 (GPa)	-41.66

Table 7. Validation of performances of the multimodal GPT-4 model. The holdout dataset over which RMSE and R<sup>2</sup> are calculated is the same as the one proposed for the validation of domain-specific multimodal models previously presented. The In-Context samples instead, belong to the training dataset, again analogous to the previous cases.

- Curtarolo, S., Hart, G. L., Nardelli, M. B., Mingo, N., Sanvito, S., and Levy, O. The high-throughput highway to computational materials design. *Nature materials*, 12(3): 191–201, 2013.
- De, S., Bartók, A. P., Csányi, G., and Ceriotti, M. Comparing molecules and solids across structural and alchemical space. *Physical Chemistry Chemical Physics*, 18(20): 13754–13769, 2016.
- Dunn, A. et al. Benchmarking materials property prediction methods: the matbench test set and automatminer reference algorithm. *Npj Comput. Mater.*, 6:138, 2020.
- Duvenaud, D. K. et al. Convolutional networks on graphs for learning molecular fingerprints. *NeurIPS*, pp. 2224–2232, 2015.
- Ganose, A. M. and Jain, A. Robocrystallographer: automated crystal structure text descriptions and analysis. *MRS Communications*, 9, 2019.
- Greeley, J., Jaramillo, T. F., Bonde, J., Chorkendorff, I., and Nørskov, J. K. Computational high-throughput screening of electrocatalytic materials for hydrogen evolution. *Nature materials*, 5(11):909–913, 2006.
- Hachmann, J. et al. The harvard clean energy project: Large-scale computational screening and design of organic photovoltaics on the world community grid. *J. Phys. Chem. Lett.*, 2(2241), 2011.
- Hong, W. T., Welsch, R. E., and Shao-Horn, Y. Descriptors of oxygen-evolution activity for oxides: a statistical evaluation. *The Journal of Physical Chemistry C*, 120(1): 78–86, 2016.
- Isayev, O., Oses, C., Toher, C., Gossett, E., Curtarolo, S., and Tropsha, A. Universal fragment descriptors for predicting properties of inorganic crystals. *Nature communications*, 8(1):15679, 2017.
- Jain, A. et al. The materials project: A materials genome approach to accelerating materials innovation. *APL Mater*, 1(011002), 2013.
- Jorgensen, J. et al. Neural message passing with edge updates for predicting properties of molecules and materials. *arXiv.org e-Print archive*, pp. arXiv:1806.01261, 2018.
- Kohn, W., Becke, A. D., and Parr, R. G. Density functional theory of electronic structure. *The journal of physical chemistry*, 100(31):12974–12980, 1996.
- Lan, Z., Chen, M., Goodman, S., Gimpel, K., Sharma, P., and Soricut, R. ALBERT: A lite BERT for self-supervised learning of language representations. *CoRR*, abs/1909.11942, 2019. URL <http://arxiv.org/abs/1909.11942>.
- LeCun, Y., Bengio, Y., and Hinton, G. Deep learning. *nature*, 521(7553):436–444, 2015.
- Lin, L.-C., Berger, A. H., Martin, R. L., Kim, J., Swisher, J. A., Jariwala, K., Rycroft, C. H., Bhowan, A. S., Deem, M. W., Haranczyk, M., et al. In silico screening of carbon-capture materials. *Nature materials*, 11(7):633–641, 2012.
- Liu, Y., Ott, M., Goyal, N., Du, J., Joshi, M., Chen, D., Levy, O., Lewis, M., Zettlemoyer, L., and Stoyanov, V. Roberta: A robustly optimized BERT pretraining approach. *CoRR*, abs/1907.11692, 2019. URL <http://arxiv.org/abs/1907.11692>.
- Massa, D., Kaxiras, E., and Papanikolaou, S. Alloy informatics through ab initio charge density profiles: Case study of hydrogen effects in face-centered cubic crystals, 2023.
- Michalski, R. S., Carbonell, J. G., and Mitchell, T. M. *Machine learning: An artificial intelligence approach*. Springer Science & Business Media, 2013.
- Montavon, G., Rupp, M., Gobre, V., Vazquez-Mayagoitia, A., Hansen, K., Tkatchenko, A., Müller, K.-R., and Von Lilienfeld, O. A. Machine learning of molecular electronic properties in chemical compound space. *New Journal of Physics*, 15(9):095003, 2013.
- O’Malley, T., Bursztein, E., Long, J., Chollet, F., Jin, H., Invernizzi, L., et al. Kerastuner. <https://github.com/keras-team/keras-tuner>, 2019.
- OpenAI, :, Achiam, J., and et al., S. A. Gpt-4 technical report, 2023.
- Pietrucci, F. and Andreoni, W. Graph theory meets ab initio molecular dynamics: atomic structures and transformations at the nanoscale. *Physical review letters*, 107(8): 085504, 2011.

- Radford, A., Kim, J. W., Hallacy, C., Ramesh, A., Goh, G., Agarwal, S., Sastry, G., Askell, A., Mishkin, P., Clark, J., Krueger, G., and Sutskever, I. Learning transferable visual models from natural language supervision. *CoRR*, abs/2103.00020, 2021. URL <https://arxiv.org/abs/2103.00020>.
- Rajan, K. Materials informatics. *Materials Today*, 8(10): 38–45, 2005.
- Ramakrishna, S., Zhang, T.-Y., Lu, W.-C., Qian, Q., Low, J. S. C., Yune, J. H. R., Tan, D. Z. L., Bressan, S., Sanvito, S., and Kalidindi, S. R. Materials informatics. *Journal of Intelligent Manufacturing*, 30:2307–2326, 2019.
- Ramprasad, R., Batra, R., Pilania, G., Mannodi-Kanakkithodi, A., and Kim, C. Machine learning in materials informatics: recent applications and prospects. *npj Computational Materials*, 3(1):54, 2017.
- Rupp, M., Tkatchenko, A., Müller, K.-R., and Von Lilienfeld, O. A. Fast and accurate modeling of molecular atomization energies with machine learning. *Physical review letters*, 108(5):058301, 2012a.
- Rupp, M., Tkatchenko, A., Müller, K.-R., and Von Lilienfeld, O. A. Fast and accurate modeling of molecular atomization energies with machine learning. *Physical review letters*, 108(5):058301, 2012b.
- Saal, E. et al. Materials design and discovery with high-throughput density functional theory: The open quantum materials database (oqmd). *JOM*, 65(1501), 2013a.
- Saal, J. E., Kirklin, S., Aykol, M., Meredig, B., and Wolverton, C. Materials design and discovery with high-throughput density functional theory: the open quantum materials database (oqmd). *Jom*, 65:1501–1509, 2013b.
- Sadeghi, A., Ghasemi, S. A., Schaefer, B., Mohr, S., Lill, M. A., and Goedecker, S. Metrics for measuring distances in configuration spaces. *The Journal of chemical physics*, 139(18), 2013.
- Schütt, K. et al. Schnet: a continuous-filter convolutional neural network for modeling quantum interactions. *NeurIPS*, 30:991–1001, 2017.
- Seko, A., Togo, A., Hayashi, H., Tsuda, K., Chaput, L., and Tanaka, I. Prediction of low-thermal-conductivity compounds with first-principles anharmonic lattice-dynamics calculations and bayesian optimization. *Physical review letters*, 115(20):205901, 2015.
- Shen, J.-X., Munro, J. M., Horton, M. K., Huck, P., Dwaraknath, S., and Persson, K. A. A representation-independent electronic charge density database for crystalline materials, 2021.
- Shih, M., Miao, J., Mills, M., and Ghazisaeidi, M. e. a. Stacking fault energy in concentrated alloys. *Nature Communications*, 12:3590, 2021.
- Summaira, J., Li, X., Shoib, A. M., Li, S., and Abdul, J. Recent advances and trends in multimodal deep learning: A review, 2021.
- Takahashi, K. and Tanaka, Y. Materials informatics: a journey towards material design and synthesis. *Dalton Transactions*, 45(26):10497–10499, 2016.
- Takamoto, S., Izumi, S., and Li, J. Teanet: Universal neural network interatomic potential inspired by iterative electronic relaxations. *Computational Materials Science*, 207: 111280, 2022.
- Torrey, L. and Shavlik, J. Transfer learning. In *Handbook of research on machine learning applications and trends: algorithms, methods, and techniques*, pp. 242–264. IGI global, 2010.
- Ward, L. and Wolverton, C. Atomistic calculations and materials informatics: A review. *Current Opinion in Solid State and Materials Science*, 21(3):167–176, 2017.
- Wilmer, C. E., Leaf, M., Lee, C. Y., Farha, O. K., Hauser, B. G., Hupp, J. T., and Snurr, R. Q. Large-scale screening of hypothetical metal–organic frameworks. *Nature chemistry*, 4(2):83–89, 2012.
- Wu, Z. et al. Moleculenet: a benchmark for molecular machine learning. *Chem. Sci.*, 9:513–530, 2018.
- Xie, T. and Grossman, J. C. Crystal graph convolutional neural networks for an accurate and interpretable prediction of material properties. *Phys. Rev. Lett.*, 120:145301, 2018a.
- Xie, T. and Grossman, J. C. Hierarchical visualization of materials space with graph convolutional neural networks. *J. Chem. Phys.*, 149:174111, 2018b.
- Xue, D., Balachandran, P., Hogden, J., Theiler, J., Xue, D., and Lookman, T. Accelerated search for materials with targeted properties by adaptive design. *Nat Commun*, 7: 11241, 2016.

## A. Appendix

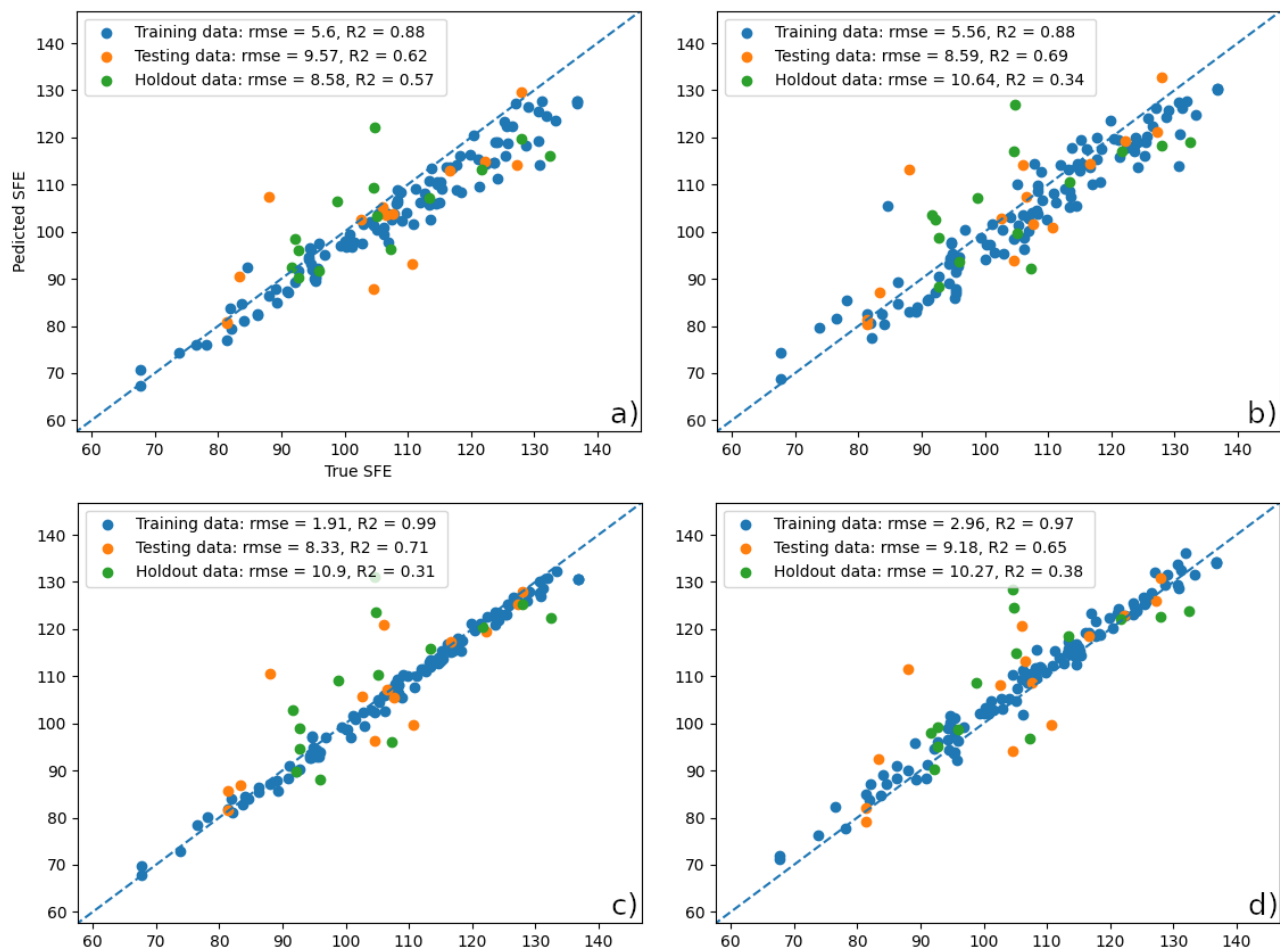


Figure 5. Reproducibility tests on the model proposed by G. Arora *et al.* (2022). Panels a)-d) present the parity plots for runs with different initialization seed.

Trial	Training		Testing		Holdout	
	RMSE	R <sup>2</sup>	RMSE	R <sup>2</sup>	RMSE	R <sup>2</sup>
#1	5.60	0.88	9.57	0.62	8.58	0.57
#2	5.56	0.88	8.59	0.69	10.64	0.34
#3	1.91	0.99	8.33	0.71	10.90	0.31
#4	2.96	0.97	9.18	0.65	10.27	0.38
#5	7.22	0.80	10.21	0.57	12.61	0.07
#6	6.78	0.82	10.28	0.56	10.78	0.32
#7	5.60	0.88	9.57	0.62	12.84	0.04
#8	4.26	0.93	8.70	0.69	10.11	0.40
#9	2.22	0.98	9.09	0.66	9.85	0.43

Table 8. Reproducibility tests on the model proposed by G. Arora *et al.* (2022). Columns 1-9 present the results for runs with different initialization seed.

Model	Param.	Training		Testing		Holdout	
		RMSE	R <sup>2</sup>	RMSE	R <sup>2</sup>	RMSE	R <sup>2</sup>
InceptionV3	6 , 0.0075	6.69	0.80	5.57	0.87	4.90	0.92
InceptionV3	6 , 0.0070	6.50	0.81	5.90	0.86	5.35	0.91
InceptionV3	6 , 0.0068	5.90	0.85	4.71	0.91	4.76	0.92
InceptionV3	6 , 0.0065	5.78	0.85	4.56	0.92	4.63	0.93

Table 9. Stability of the fine-tuned performances of the proposed model towards a small change in learning rate and with no fixed seed.

Model	Param.	Training		Testing		Holdout	
		RMSE	R <sup>2</sup>	RMSE	R <sup>2</sup>	RMSE	R <sup>2</sup>
InceptionV3	6 , 0.0070	6.50	0.81	5.90	0.86	5.35	0.91
InceptionV3	6 , 0.0070	5.19	0.88	3.72	0.94	4.05	0.95

Table 10. Stability of the fine-tuned performances of the proposed model towards a change in computing machine and with no fixed seed.

Collected properties
nsites
nelements
volume
density
density_atomic
uncorrected_energy_per_atom
energy_per_atom
formation_energy_per_atom
energy_above_hull
equilibrium_reaction_energy_per_atom
band_gap
efermi
total_magnetization
total_magnetization_normalized_vol
total_magnetization_normalized_formula_units
num_magnetic_sites
num_unique_magnetic_sites
k_voigt
k_reuss
k_vrh
g_voigt
g_reuss
g_vrh
universal_anisotropy
homogeneous_poisson

Table 11. Collected properties of the crystals from the Materials Project database.

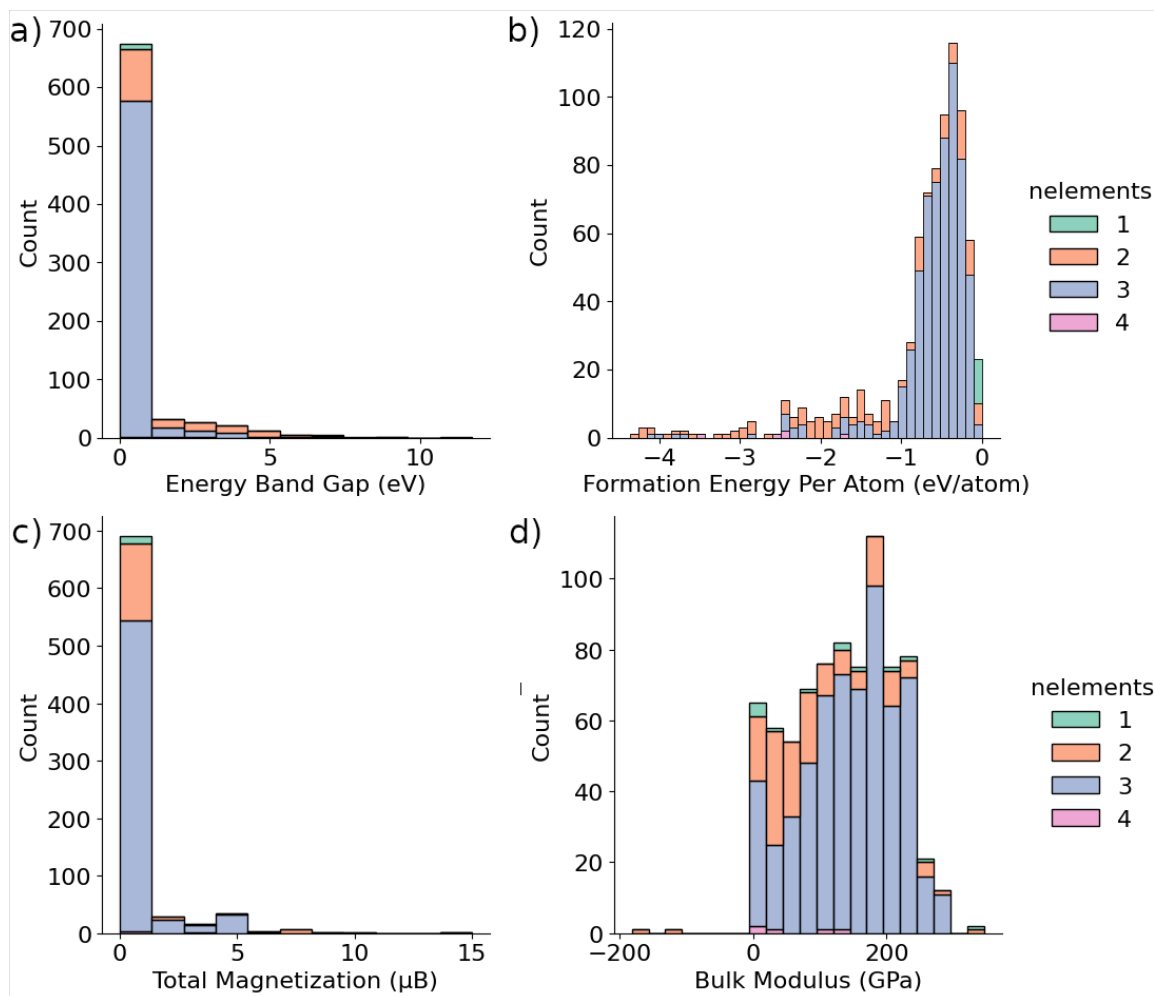


Figure 6. Distribution of the samples focusing on a) energy band gaps, b) formation energies per atom, c) bulk moduli and d) total magnetization properties, as collected from Materials Project database. The colors palette follows the number of elements present in the crystal composition.

Target	Measure	ALBERT								
		Single			Key			Most		
		Tr	Te	H	Tr	Te	H	Tr	Te	H
$E_{\text{BG}}$	RMSE (eV)	0.03	0.1	0.11	0.03	0.05	0.09	0.04	0.05	0.1
	$R^2$	0.90	0.42	0.27	0.93	0.86	0.53	0.88	0.82	0.41
$E_{\text{F}}$	RMSE (eV/atom)	0.04	0.12	0.12	0.06	0.08	0.08	0.03	0.05	0.07
	$R^2$	0.95	0.42	0.53	0.89	0.75	0.76	0.97	0.89	0.80
$M_{\text{tot}}$	RMSE ( $\mu\text{B}$ )	0.04	0.06	0.10	0.03	0.05	0.1	0.06	0.06	0.12
	$R^2$	0.75	0.38	0.49	0.85	0.67	0.53	0.57	0.47	0.25
B	RMSE (GPa)	0.05	0.09	0.08	0.04	0.06	0.06	0.03	0.06	0.05
	$R^2$	0.89	0.62	0.69	0.93	0.80	0.84	0.94	0.85	0.87

Table 12. Comparison between the performances of the custom combined model of InceptionV3 and ALBERT for regression of crystal properties using images and text, in the case of single word (crystal composition), key words (composition and bond lengths) and of most words allowed by the model. The target properties for regression are: energy band gap ( $E_{\text{BG}}$ ), formation energy ( $E_{\text{F}}$ ), total magnetization ( $M_{\text{tot}}$ ), bulk modulus (B). Performances are evaluated in terms of RMSE and  $R^2$  measures, for training (Tr), testing (Te), and Holdout (H) sets.

		roberta-base, Single					
Target	Measure	Pre-Trained (images)			Finetuning (image)		
		Tr	Te	H	Tr	Te	H
$M_{\text{tot}}$	RMSE ( $\mu\text{B}$ )	0.08	0.07	0.13	0.08	0.07	0.12
	$R^2$	0.1	0.18	0.18	0.14	0.32	0.29
		Pre-Trained (images+text)			Finetuning (images+text)		
$M_{\text{tot}}$	RMSE ( $\mu\text{B}$ )	0.04	0.06	0.11	0.02	0.04	0.09
	$R^2$	0.82	0.36	0.42	0.94	0.75	0.57

Table 13. Example of change in regression performances during the different stages of the entire transfer learning procedure in the custom multimodal model, when composed by InceptionV3 and RoBERTa. The results refer to the case of using a Single word in the text dataset (crystal composition). Performances are evaluated in terms of RMSE ( $\mu\text{B}$ ) and  $R^2$  measures, for training (Tr), testing (Te), and Holdout (H) sets.

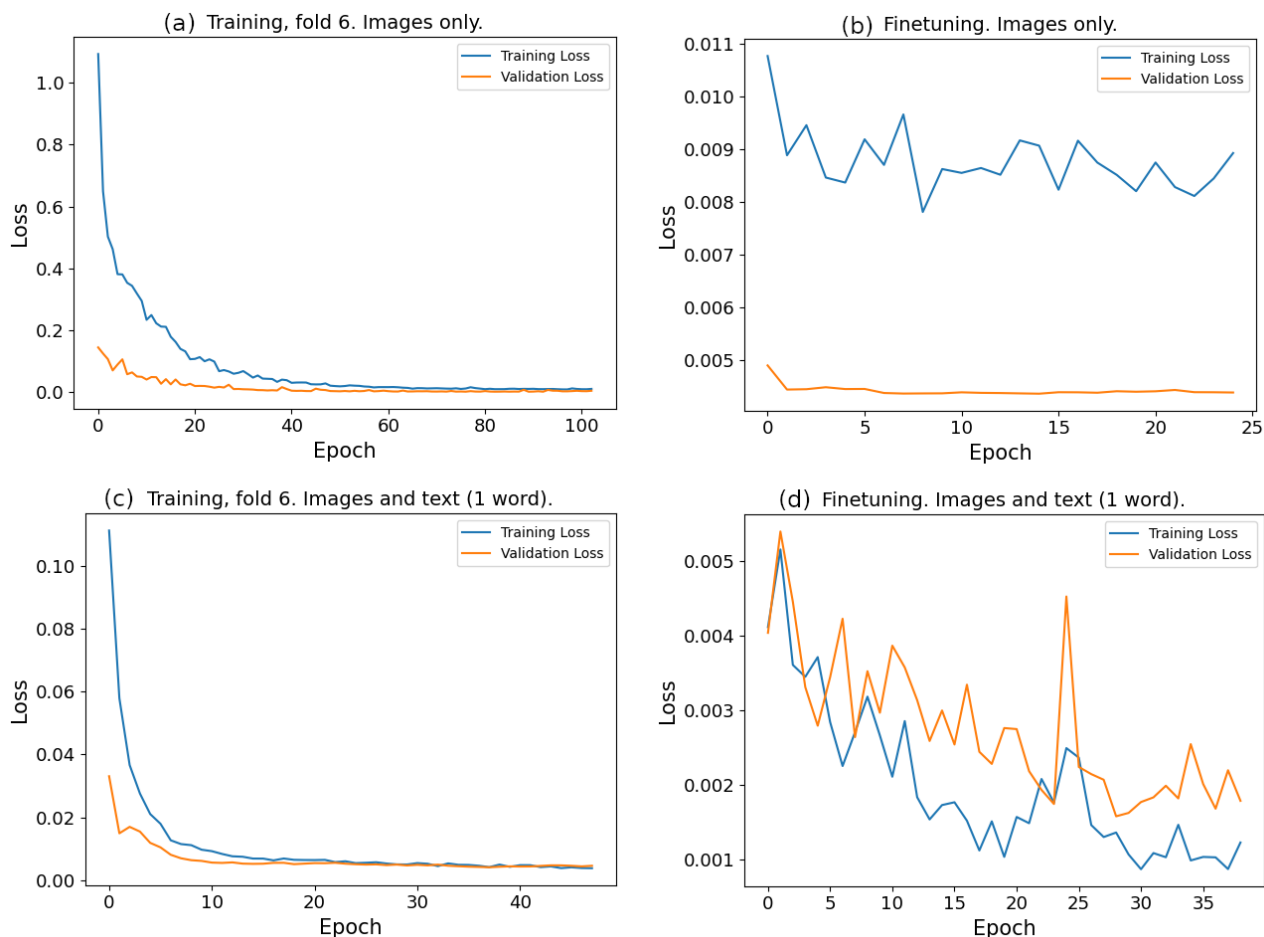


Figure 7. Learning curves during the different stages of the entire transfer learning procedure in the custom multimodal model, when composed by InceptionV3 and RoBERTa. The results refer to the case of using a Single word in the text dataset (crystal composition).